

AD-A161 651

DEVELOPMENT OF A GEOMAGNETIC STORM PREDICTION SCHEME

1/1

(U) ALASKA UNIV FAIRBANKS GEOPHYSICAL INST

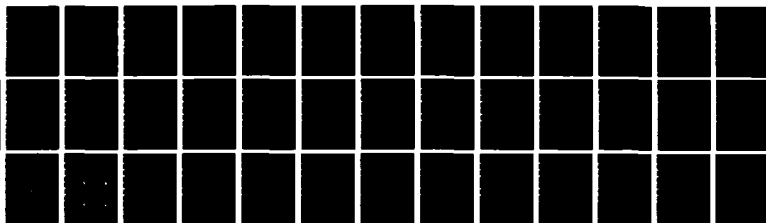
S I AKASOFU ET AL JUN 85 AFGL-TR-85-0152

UNCLASSIFIED

F19628-82-K-0035

F/G 8/14

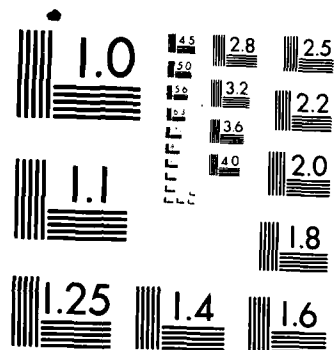
NL



END

FILMED

DTIC



MICROCOPY RESOLUTION TEST CHART
NATIONAL BUREAU OF STANDARDS-1963-A

AD-A161 651

12

AFGL-TR-85-0152

DEVELOPMENT OF A GEOMAGNETIC STORM PREDICTION SCHEME -
PHASE I

S.-I. Akasofu
C. F. Fry

Geophysical Institute
University of Alaska
Fairbanks, Alaska 99701

June 1985

Final Report
23 February 1982 - 23 April 1985

APPROVED FOR PUBLIC RELEASE; DISTRIBUTION UNLIMITED

AIR FORCE GEOPHYSICS LABORATORY
AIR FORCE SYSTEMS COMMAND
UNITED STATES AIR FORCE
HANSCOM AFB, MASSACHUSETTS 01731

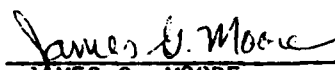
DTIC FILE COPY

46

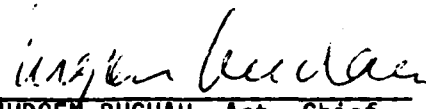
NOV 20 1985

11 20-85 019

"This technical report has been reviewed and is approved for publication"




JAMES G. MOORE
Contract Manager
Ionospheric Effects Branch



JURGEN BUCHAU, Act. Chief
Ionospheric Effects Branch
Ionospheric Physics Division

FOR THE COMMANDER



ROBERT A. SKRIVANEK
Director
Ionospheric Physics Division

This report has been reviewed by the ESD Public Affairs Office (PA) and is releasable to the National Technical Information Service (NTIS).

Qualified requestors may obtain additional copies from the Defense Technical Information Center. All others should apply to the National Technical Information Service.

If your address has changed, or if you wish to be removed from the mailing list, or if the addressee is no longer employed by your organization, please notify AFGL/DAA, Hanscom AFB, MA 01731. This will assist us in maintaining a current mailing list.

Unclassified

SECURITY CLASSIFICATION OF THIS PAGE (When Data Entered)

REPORT DOCUMENTATION PAGE		READ INSTRUCTIONS BEFORE COMPLETING FORM
1. REPORT NUMBER AFGL-TR-85-0152	2. GOVT ACCESSION NO. AD A161657	3. RECIPIENT'S CATALOG NUMBER
4. TITLE (and Subtitle) DEVELOPMENT OF A GEOMAGNETIC STORM PREDICTION SCHEME - PHASE I		5. TYPE OF REPORT & PERIOD COVERED Final Report, 23 February 1982 - 23 April 1985
		6. PERFORMING ORG. REPORT NUMBER
7. AUTHOR(s) S.-I. Akasofu C. F. Fry		8. CONTRACT OR GRANT NUMBER(s) F19628-82-K-0035
9. PERFORMING ORGANIZATION NAME AND ADDRESS Geophysical Institute University of Alaska Fairbanks, Alaska 99701		10. PROGRAM ELEMENT, PROJECT, TASK AREA & WORK UNIT NUMBERS 63703F 464308AB
11. CONTROLLING OFFICE NAME AND ADDRESS Air Force Geophysics Laboratory Hanscom A.F.B., Massachusetts 01731 Monitor/James G. Moore/LIS		12. REPORT DATE June 1985
		13. NUMBER OF PAGES 40
14. MONITORING AGENCY NAME & ADDRESS (if different from Controlling Office)		15. SECURITY CLASS. (of this report) unclassified
		15a. DECLASSIFICATION/DOWNGRADING SCHEDULE
16. DISTRIBUTION STATEMENT (of this Report) Approved for public release; distribution unlimited		
17. DISTRIBUTION STATEMENT (of the abstract entered in Block 20, if different from Report)		
18. SUPPLEMENTARY NOTES		
19. KEY WORDS (Continue on reverse side if necessary and identify by block number) Geomagnetic Storm Forecasting Solar Wind Magnetosphere Interaction; Interplanetary Field Magnetic Modeling Polar Cap Convection		
20. ABSTRACT (Continue on reverse side if necessary and identify by block number) Geomagnetic and auroral disturbances cause significant interference on many electrical systems. Therefore, it is essential to develop a reliable geomagnetic and auroral storm prediction scheme. Present geomagnetic storm prediction schemes rely entirely on statistical results, so that they can hardly provide quantitative information on the intensity of a geomagnetic storm caused by a particular solar event, it is for this reason that we have been developing a first generation numerical prediction scheme.		

DD FORM 1473
1 JAN 73EDITION OF 1 NOV 65 IS OBSOLETE
S/N 0102 LF 014-6601

Unclassified

SECURITY CLASSIFICATION OF THIS PAGE (When Data Entered)

20. Abstract (cont.)

The scheme consists of two major computer codes which in turn consist of a large number of subroutine codes and of empirical relationships. First of all, when a solar flare occurs, six flare parameters are determined as the input data set for the first code which is devised to show the simulated propagation of solar wind disturbances in the heliosphere to a distance of 2 AU. Thus, one can determine the relative location of the propagating disturbances with the earth's position. The solar wind speed (V) and the three interplanetary magnetic field (IMF) components (B_x , B_y , B_z or B , θ , ϕ) are then computed as a function of time at the earth's location or any other desired (space probe) locations. These quantities in turn become the input parameters for the second major code which computes first the power (ϵ) of the solar wind-magnetosphere dynamo as a function of time. The power thus obtained and the three IMF components can be used to compute or infer: (i), the predicted geometry of the auroral oval; (ii), the cross-polar cap potential; (iii), the two geomagnetic indices AE and Dst; (iv), the total energy injection rate into the polar ionosphere; (v), the atmospheric temperature, etc.

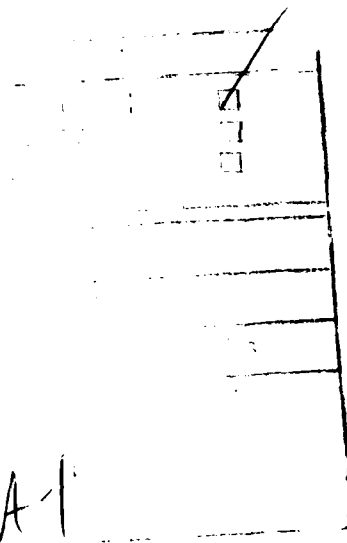
At the present time, the weakest part of the scheme arises from the fact that causes of changes of the IMF B_z (or θ) component are not well understood. Further, several empirical relationships are incorporated in the present scheme in the second major code. Thus, there are still a number of solar and geomagnetic storm features which require theoretical studies and proper modeling efforts to eventually replace the empirical relationships by theoretical ones, as our understanding of solar-terrestrial physics advances.

TABLE OF CONTENTS

INTRODUCTION	1
CAUSE OF GEOMAGNETIC STORMS AND AURORAL ACTIVITY	1
DEFINITION OF THE PREDICTION OF GEOMAGNETIC STORMS	1
NEED FOR NUMERICAL PREDICTION SCHEMES	2
KEY ELEMENT IN THE FIRST GENERATION PREDICTION SCHEME	5
A FIRST GENERATION GEOMAGNETIC STORM PREDICTION SCHEME	6
A CAUSE OF THE IMF B_z VARIATIONS	13
OUTPUTS	18
SECOND GENERATION SCHEME	27
CONCLUDING REMARKS	32
REFERENCES	33

LIST OF FIGURES

- | | |
|--|----|
| 1.1 Histogram of the transit time of solar flare-induced disturbances to the earth. | 3 |
| 1.2 Maximum values of the Dst decrease for a large number of geomagnetic storms as a function of the central meridian distance of the responsible solar flares. | 4 |
| 2.1 Numerical geomagnetic storm prediction scheme in the block-diagram form. | 7 |
| 3.1 Successive frames showing schematically, the distortion of coronal magnetic field lines due to a hypothetical coronal transient event. | 14 |
| 3.2 Meridional plane view of the solar source surface showing the kinematic method of tracing the field line associates with a poleward moving footpoint. | 16 |
| 3.3 Top: Schematic showing the steepening of IMF field line configuration as the kink propagates outward. Velocity $V_2 > V_1$. Bottom: Schematic snapshots of a field line segment at successive times as it propagates outward. | 17 |



1. Introduction

1.1 Cause of Geomagnetic Storms and Auroral Activity

Geomagnetic storms and auroral activity are caused by a large-scale electrical discharge process surrounding the earth. The magnetic fields produced by the discharge currents are identified as the geomagnetic storm fields (namely, a magnetic manifestation). The aurora is an optical manifestation of the discharge process which is caused by collisions of discharge-current carrying electrons with the polar upper atmospheric atoms and molecules.

1.2 Definition of the Prediction of Geomagnetic Storms

During a geomagnetic storm, an intense Van Allen belt is formed near the earth. The belt carries about one million amperes of electric currents, and is called the ring current belt or the storm-time Van Allen belt. The ring current produces a southward directed field in low latitudes in space between the earth's surface and the inner boundary of the belt. The magnetic field of the ring current is quantified by the geomagnetic index Dst.

A pair of concentrated currents, called the auroral electrojets, are also generated in the polar ionosphere. The total current intensity of the electrojets is of the order of a few million amperes. They cause intense and complicated magnetic fields in the auroral oval and its vicinity. The magnetic fields produced by this current system are quantified by the geomagnetic index AE. The AE index can be considered as a complementary index for auroral activity.

The geomagnetic storm intensity is thus parameterized and quantified by these two geomagnetic indices, AE and Dst. Therefore, a modern geomagnetic prediction scheme should be able to predict AE and Dst as a function of time t

within several hours of a major solar event; note that other complementary indices, such as Kp and ap indices, are derivable from the AE index.

In addition to the geomagnetic indices, several other magnetospheric and ionospheric quantities should be predicted by a modern storm prediction scheme. Some of them are:

- (i) Geometry and size of the open region polar cap and the auroral oval.
- (ii) Cross-polar cap potential Φ_{pc} .
- (iii) Total energy injection rate into the polar ionosphere.
- (iv) Increase of the upper atmospheric temperature ΔT_{∞} .
- (v) Electron density profile in the polar ionosphere.

1.3 Need for Numerical Prediction Schemes

In the past, the geomagnetic storm prediction has entirely depended on statistical results. Two examples of such statistical results are shown in Figures 1.1 and 1.2 (Akasofu and Chapman, 1972). Figure 1.1 shows the time lapse from flare onset to storm onset (the time of ssc). One can see that the lapse time is about 40 hours on the average, but it ranges from about 20 hours to 60 hours. Therefore, there is a great uncertainty in predicting the onset time of a geomagnetic storm after a flare. Figure 1.2 shows the central meridian dependence of the maximum Dst value attained by a number of storms. One can see that there is a clear dependence of the maximum possible Dst on the central meridian distance. In particular, except for one event, all major storms [$Dst > 200Y (= nT)$] are caused by flares which occurred within 30° of the central meridian distance. Such a tendency is important in predicting the maximum intensity of geomagnetic storms. However, not all central meridian flares produce large Dst storms. In Figure 1.2, the Dst values range from 0

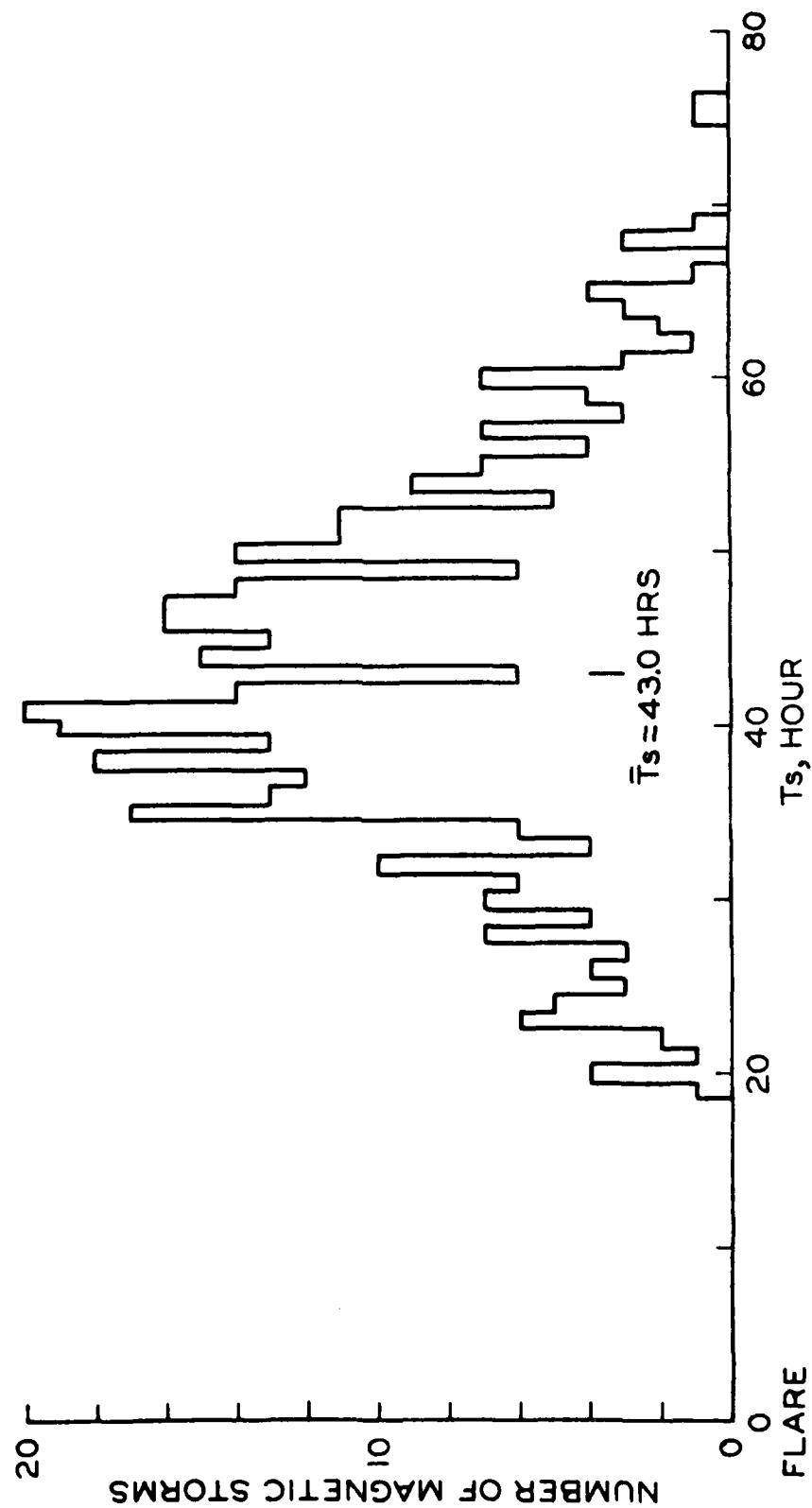


Fig. 1.1. Histogram of the transit time of solar flare-induced disturbances to the earth.

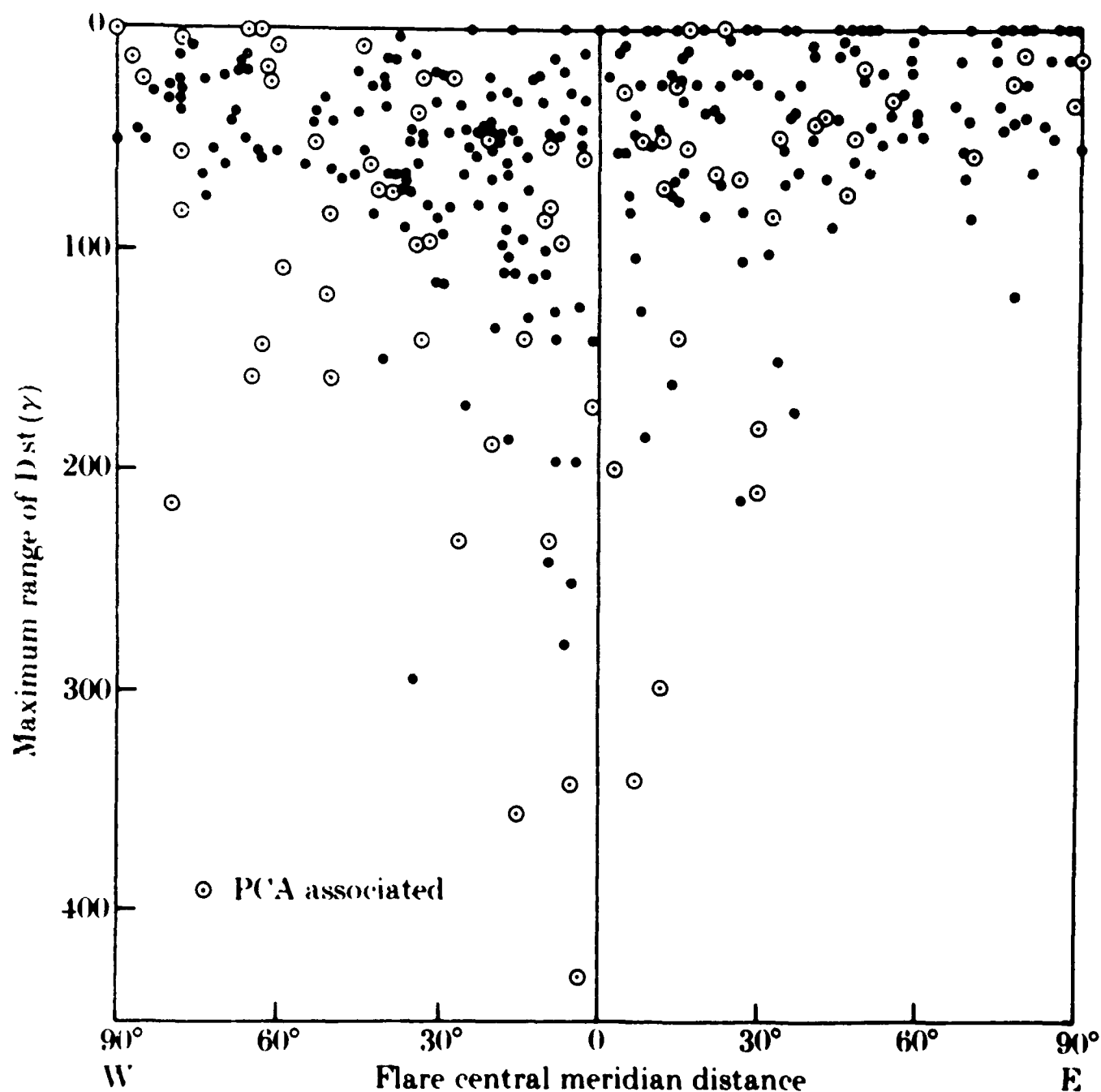


Fig. 1. Maximum values of the Dst decrease for a large number of geomagnetic storms as a function of the central meridian distance of the responsible solar flares.

to 400 nT within the central meridian range of $\pm 20^\circ$, so that one can provide only the largest possible Dst value for a given flare by knowing its central meridian distance. For this reason, there is, at present, no way to predict the time-development of the Dst index for a given flare. Therefore, one must develop a numerical scheme in predicting $AE(t)$, $Dst(t)$, the geometry of the oval, $\Phi_{pc}(t)$, $U_I(t)$, ΔT_∞ , etc.

1.4 Key Element in the First Generation Prediction Scheme

The key element which has made the numerical prediction of the intensity of geomagnetic storms and auroral activity possible is that we have succeeded in identifying the solar wind quantities which are related to the power ϵ for the auroral discharge process or the power of the solar wind-magnetosphere dynamo (Perreault and Akasofu, 1978; and Akasofu, 1981). It is given by

$$\epsilon = VB^2 \sin^4 \left(\frac{\theta}{2} \right) l_o^2 \quad (1)$$

where

V = the solar wind speed

B = the solar wind magnetic field magnitude

θ = the polar angle of the solar wind magnetic field vector

l_o = constant (~ 7 earth radii)

A tentative criteria for most systems which utilize the polar ionosphere are:

- $\epsilon < 10^5$ Mwatt ($< 10^{18}$ erg/sec) - Normal operation
- $\epsilon \sim 5 \times 10^5$ Mwatt ($\sim 5 \times 10^{18}$ erg/sec) - Require alert
- $\epsilon \sim 10^6$ Mwatt ($\sim 10^{19}$ erg/sec) - Prepare for system failure
- $\epsilon > 5 \times 10^6$ Mwatt ($\sim 5 \times 10^{19}$ erg/sec) - System failure

Therefore, the success of the prediction will depend on the accuracy of predicting the power $\epsilon(t)$ as a function of time within several hours of a major solar activity.

2. A First Generation Geomagnetic Storm Prediction Scheme

Figure 2.1 shows our first generation prediction scheme in the form of a block diagram. It can be divided into two parts, A and B.

Part A: Prediction of Disturbed Solar Wind Quantities

The first step of the prediction of geomagnetic storms and thus of the power $\epsilon(t)$ is reduced to the prediction of solar wind quantities $V(t)$, $B(t)$ and $\epsilon(t)$ (or $V(t)$, $B_x(t)$, $B_y(t)$, $B_z(t)$) in equation (1). Our first generation scheme is partly based on the method developed by Hakamada and Akasofu (1982) and Akasofu et al. (1983). This method provides a first order construction, temporally and spatially, of flare-generated shocks. It does not simulate the other dynamic, thermodynamic properties that can only be found from the MHD equations, but those quantities are not essential for the geomagnetic storm prediction. There have already been a number of simulation studies of solar wind disturbances which are based on numerical solutions of the MHD equations (cf. Blanton et al., 1981; Gislason et al., 1984). However, a full three-dimensional MHD simulation has not been developed yet for our purpose. Fortunately, it is possible to 'calibrate' our kinematic method with those three- and two-dimensional MHD simulations (Olmsted and Akasofu, 1985), so that the results should be reasonably consistent with the MHD results. In the following, a brief explanation of the codes is given.

GEOMAGNETIC STORM PREDICTION SCHEME

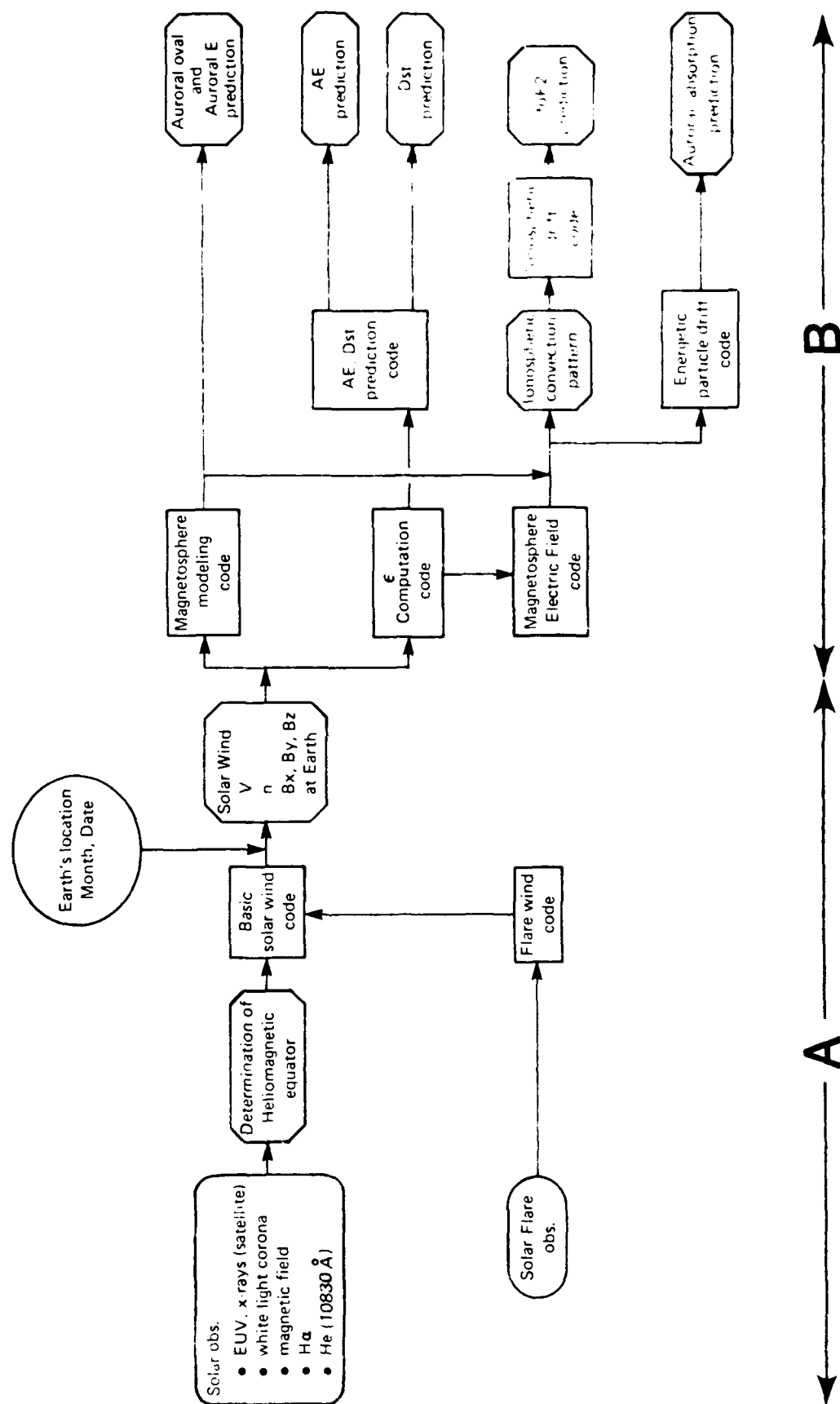


Fig. 2.1. Magnetospheric storm prediction scheme in the block diagram form.

(i) Basic background solar wind

This code sets up the background solar wind conditions into which disturbances caused by a major solar event will be introduced. In the present scheme, the background solar wind flow can be specified by knowing the location of the magnetic equator in heliographic coordinates and the latitudinal (magnetic) variations of the solar wind speed, both on the so-called 'source surface' (a spherical surface of radius of $r_s = 2.5$ solar radii).

Magnetic equator

The location of the magnetic equator (or the so-called neutral line) on the source surface plays a crucial role in modeling the background solar wind flow. It is provided by the Stanford Solar Observatory, Stanford University, every 27 days, namely after each Carrington Rotation. Therefore, the location of the magnetic equator can be updated every 27-day interval. The Stanford data also provides the magnetic field intensity B on the source surface and the intensity B_p at the magnetic pole.

Latitudinal variations of the solar wind speed

The latitudinal variation of the solar wind can be approximately expressed by:

$$v = v_0 + (v_1 - v_0) (1 - \cos^\alpha \lambda_m)$$

where $\lambda_m = \sin^{-1} (B/B_p)$

The three parameters α , v_0 and v_1 in the n th year of the sunspot cycle are tentatively given in the following table (Fry, 1985). In the scheme, the three parameter values are automatically selected by specifying the year in A.D.

/Year	1st	2nd	3rd	4th	5th	6th	7th	8th	9th	10th	11th
α	32	16	8	4	3	3	4	6	12	20	32
v_0	270	270	270	270	270	270	270	270	270	270	270
v_1	700	680	670	650	650	650	660	670	680	690	700

Background code

The background code provides the solar wind speed V , density n and the three components B_x , B_y and B_z (or the magnitude B , latitude angle θ and azimuth angle ϕ ; $\theta = 90^\circ - \lambda$ at the location of the earth for a 27-day period and/or at any other location in the heliosphere for space probes. Two displays are prepared for the background solar wind information.

OUTPUT 1

The first is the location of the magnetic equator in Carrington longitude-latitude coordinates, together with some iso-B contours. As an example, it is assumed that the magnetic equator in this coordinate system is given by a sinusoidal curve during the Carrington Rotation 1836 (November 23 - December 19, 1990). The projected location of the earth on the source surface on December 10, 1990 is indicated by *.

OUTPUT 2

The second is the predicted 27-day variation of the solar wind speed and the density, the IMF magnitude B and the two angles θ and ϕ at the earth's location, without flares or other solar activities, for the same Carrington Rotation period, November 23 - December 19, 1990. Note that since the magnetic equator is sinusoidal in the Carrington coordinate system in this illustrative example, two maxima of the solar wind speed are observed at the earth. Note also a sharp change of the angle ϕ either from 135° to 315° or from 315° to 135° , indicating the crossing of the solar current sheet (or the so-called 'sector-boundaries').

For an accurate storm prediction, Output 1 and Output 2 should be continuously updated, since flare-induced disturbances will be superposed on the background solar wind flow.

(ii) Solar Flare Code

Solar observatories provide the following information on a solar flare:

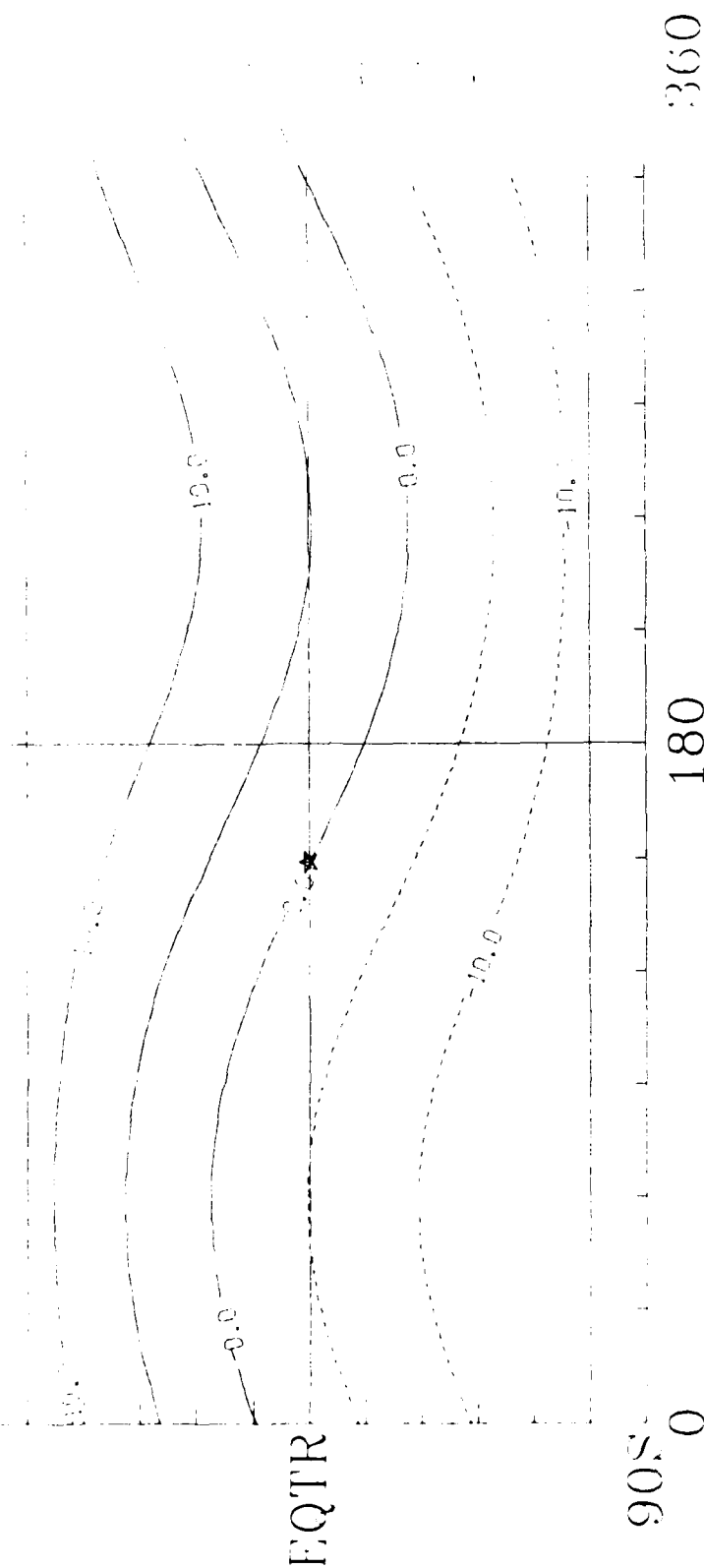
- . Start time
- . Time of maximum flare intensity
- . Latitude (N, S)
- . Central meridian distance (E, W)
- . Importance (0, 1, 2, 3, 4)
- . End time

In the flare code, each flare is described by the following six parameters.

- | | |
|---------------------|--|
| . Start time | T_F : Flare start time minus simulation start time, in hours. |
| . Latitude | ϕ_F : Flare latitude (N = +, S = -). |
| . Longitude | λ_F : Flare longitude (W = +, E = 1) earth's longitude. |
| . Initial speed | V_F : Flare speed at source surface at maximum epoch. See Table 1. |
| . Area σ_F : | Aerial extent of flare, standard deviation for gaussian spatial extent on source surface. See following Table. |
| . Duration | τ_F : Flare time constant. |

The first three parameters T_F , ϕ_F and λ_F are the same as the observed start time, latitude and central meridian distance. Based on

90%



Output 1

CONTOUT FROM -10.000 TO 10.000 CONTOUT INTERVAL OF 5.0000 PT13.31E -13.607

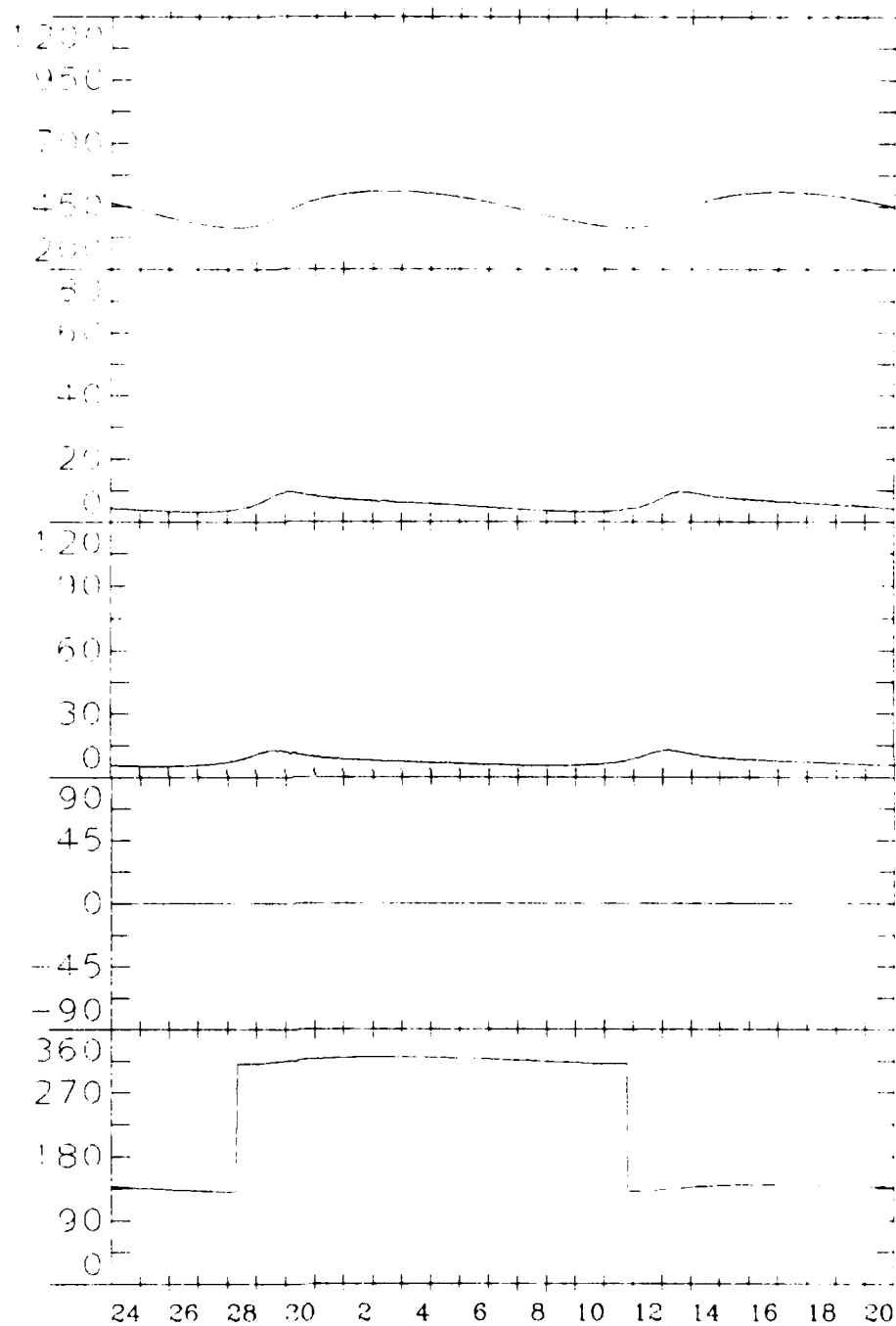
VEL
(Km/Sec)

Dens
(CM⁻³)

/B/
(nT)

Θ
(°)

Φ
(°)



NOV., 1990

DEC., 1990

Output 2

the observed Importance and Brilliance, V_F and σ_F are chosen from the following tentative conversion table. In the scheme, as one specifies the flare intensity, this procedure is automatically accomplished. The flare time constant τ_F is tentatively taken to be ten times of flare duration (see Section 5(B)).

Conversion from flare Importance and Brilliance to V_F and σ_F .
Importance/Brilliance V_F (km/sec) $\sigma_F(^{\circ})$

0F	200	20
0N	300	30
0B	400	40
1F	400	30
1N	600	40
1B	800	50
2F	500	30
2N	800	50
2B	1200	70
3F	700	30
3N	1100	50
3B	1500	70
4F	800	40
4N	1200	60
4B	1600	80

Part B: Prediction of Geomagnetic Disturbances

The second part (B) of the prediction scheme takes the outputs of the first part (A) as the input. As the solar wind speed (V) and the three interplanetary magnetic components (B_x , B_y , B_z) become available as a function of time, it is possible to estimate the auroral discharge power ϵ as a function of time from equation (1). On the basis of V , $B(B_x, B_y, B_z)$ and ϵ thus determined, the following quantities can be computed.

(i) Open region (auroral oval) geometry

The oval geometry code takes the power ϵ as the input and determines the geometry of the poleward boundary of the auroral oval in magnetic latitude - local time coordinates. This code is based on a study of the dependence of the polar cap (the open field line region) on the IMF by Akasofu and Roederer (1984).

(ii) Cross-polar potential

The cross-polar cap potential Φ_{pc} is found to be proportional to $\sqrt{\epsilon}$ (Reiff et al., 1981); it is given by $\Phi_{pc} = 30 + 0.006\sqrt{\epsilon'}$ where $\epsilon' = VB^2 \sin^4(\theta/2)$ ($10^4 \text{ nT}^2 \text{ km/sec}$). Combining this empirical result with the auroral oval geometry code, one can also infer the distribution of the electric field in the polar regions. We also have the option of using

the empirical relationship between ϕ_{pc} and AE, determined by Ahn et al. (1984); it is given by ϕ_{pc} (KV) = $36 + 0.089 \text{ AE(nT)}$ or ϕ_{pc} (KV) = $4.2 \times 10^{-17} \epsilon(\text{erg/sec})$.

(iii) AE, Dst prediction

This code takes the power ϵ as the input and predicts the AE and Dst indices. The AE index is computed on the basis of an empirical relationship between ϵ and AE, $\text{AE(nT)} = 600[\tanh(\log_{10} \epsilon - 18.9)]^{2/3} + 650$. The Dst(nT) index is computed from equation $4 \times 10^{20} (\partial \text{Dst} / \partial t + \text{Dst} / \tau_R) = 0.7\epsilon$, where τ_R is the lifetime of ring current particles (Akasofu, 1982).

(iv) Magnetospheric convection

This code takes the power ϵ as the input and determines the convection pattern of magnetospheric plasma over the entire polar ionosphere. It is assumed that the cross-polar potential drop ϕ_{pc} is applied to the open field line region determined in (ii).

(v) Total energy injection rate U_I into the polar ionosphere

This estimate is based on the formula, U_I (watt) = $2.9 \times 10^8 \text{ AE(nT)}$ (or $2.9 \times 10^{15} \text{ AE(nT) erg/sec}$); see Ahn et al. (1984).

(vi) Increased temperature in the thermosphere

This estimate is based on the formula, $\Delta T_{\infty}(\text{K}) = e^x - 300$ where $x = 0.45 \ln (\epsilon(\text{erg}) / 10^{17} + 0.3) + 5.0$. This empirical relation was obtained by Prölss (1985).

3. A Cause of the IMF B_z Variations

We represent schematically the sequence of magnetic field configurations which might result from a particular type of coronal disturbance. The corona is assumed to initially have a dipolar magnetic field configuration. Figure 3.1 shows schematically a series of field configurations at successive time steps. As a coronal transient occurs in the lower solar atmosphere, the magnetic field lines are forced to move poleward. As a result, the intersecting points of the field lines on the source surface, at $r_s = 2.5$ solar radii, move poleward. This induces a polar component in the field line orientation outward from the source surface, and a polar IMF vector component results. The distortion of the field lines propagates outward. As the dis-

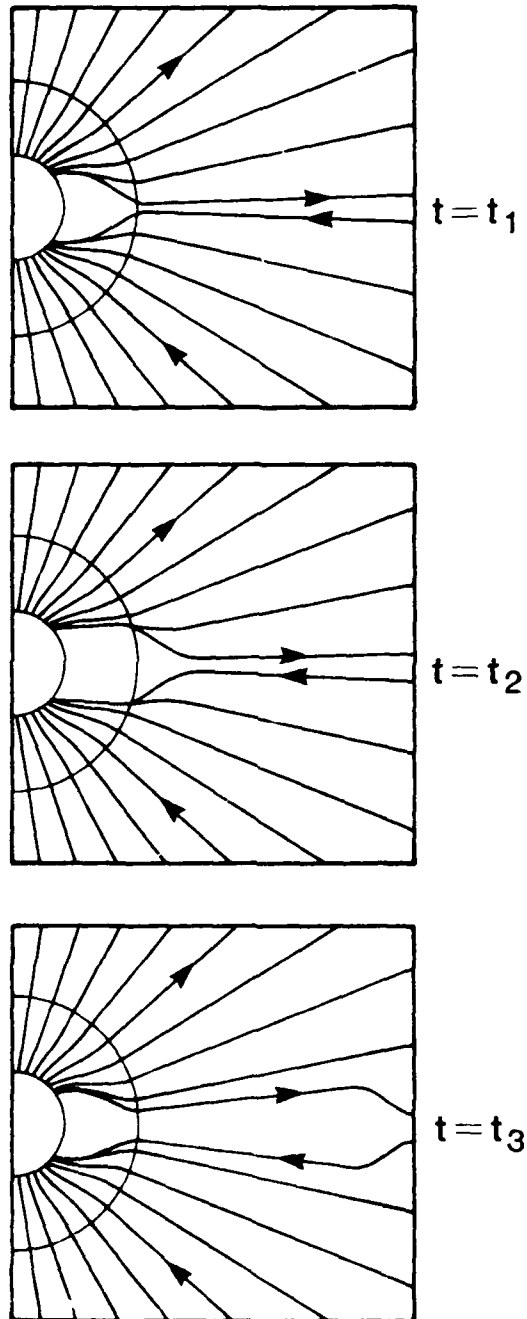


Fig. 3.1. Successive frames showing schematically, the distortion of coronal magnetic field lines due to a hypothetical coronal transient event.

turbance moves outward past the source surface, the field lines gradually return to their original latitudes on the source surface. Since the field lines are imbedded in the outflowing plasma, the distortion continues to propagate outward beyond the source surface.

Figures 3.2 and 3.3 represent the meridional plane view of the solar source surface in the case of a poleward motion of the field lines. The kinematic code traces the field line as follows. At time $t = t_1$, the sun emits a fluid parcel, or "particle" (position 1). At a later time, $t = t_2$, the emitted particle has moved radially outward to position 2. The source region (which emitted the particle) has moved to position 3 by the time $t = t_2$. The region emits a second particle at position 3. Particles at positions 2 and 3 are connected by the same field line. This situation is similar to the streamline of water formed by suddenly moving a garden hose upward. The resulting kink in the streamline (and the magnetic field line) propagates outward at the fluid flow speed. The meridional velocity must be comparable to the radial velocity to induce a β angle of about 45° .

For a solar wind speed on the source surface of about 50 km s^{-1} , the polar motion required to allow B_z comparable to B_x in the IMF is also about 50 km s^{-1} . This is because even though the radial speed v_r is increasing outward from the sun due to acceleration of the coronal plasma, v_r is also increasing outward at all latitudes. In this case, the meridional field line kink will experience a steepening in β angle as it propagates outward, since the background solar wind velocity increases away from the magnetic neutral line.

The field line location on the source surface is represented by its magnetic latitude, which is now allowed to vary according to the equation,

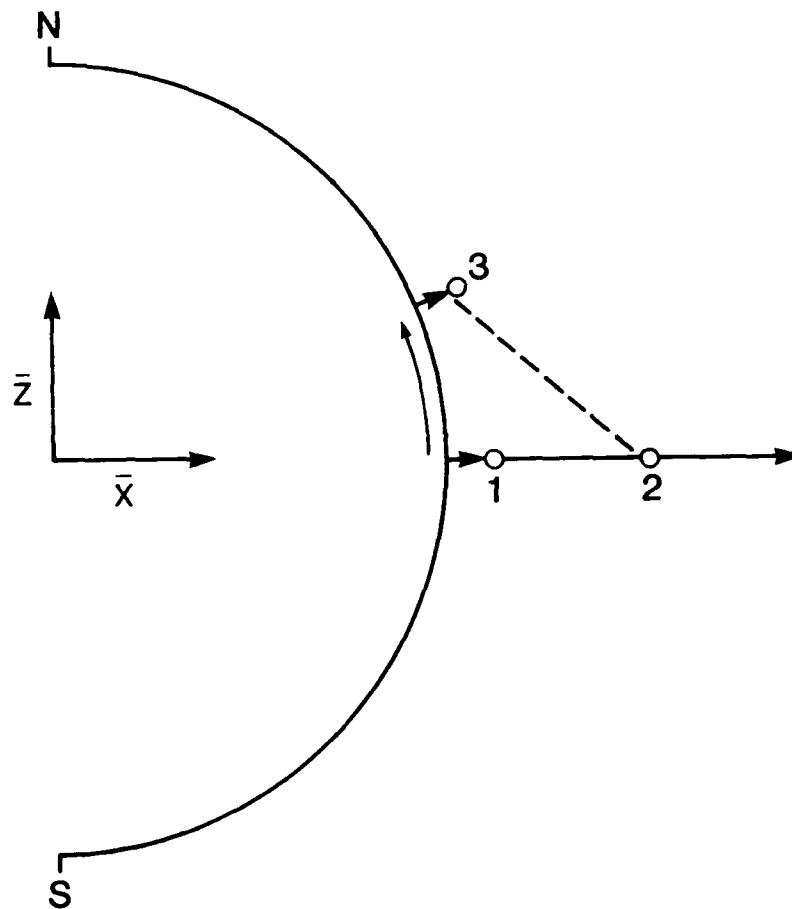


Fig. 3.2. Meridional plane view of the solar source surface showing the kinematic method of tracing the field line associated with a poleward moving footpoint.

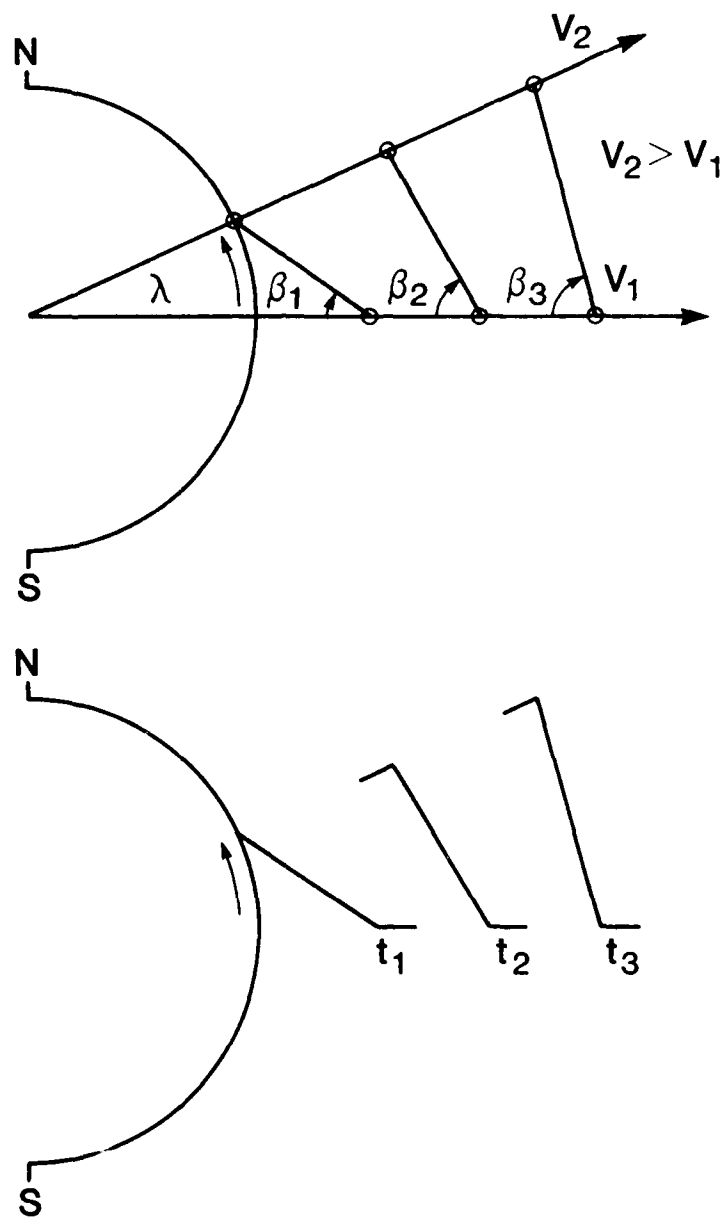


Fig. 3.3. Top: Schematic showing the steepening of IMF field line configuration as the kink propagates outward. Velocity $V_2 > V_1$. Bottom: Schematic snapshots of a field line segment at successive times as it propagates outward.

$$\lambda_m = \lambda_{mo} - \Delta\lambda_m$$

$$\Delta\lambda_m = .5\lambda_{mo} \left(\frac{t-t_F}{\tau_F}\right) \exp(-R^2/\sigma^2) \exp\left[1 - \left(\frac{t-t_F}{\tau_F}\right)\right]$$

where

λ_{mo} = magnetic latitude for the dipole case, or approximately, $\lambda_{mo} = \chi \sin(\phi - \phi_0)$.

The background magnetic field configuration, λ_{mo} , in these cases is that of a dipole field with a tilt of $\chi = 20^\circ$ with respect to the rotational axis. At observation longitude = 0° , the β variation is similar both above and below the current sheet. The observation point is above the current sheet when the ϕ angle is about 135° , and below when $\phi \sim 135^\circ$. The abrupt change in ϕ angle signals the current sheet passage, or the so-called "sector boundary crossing."

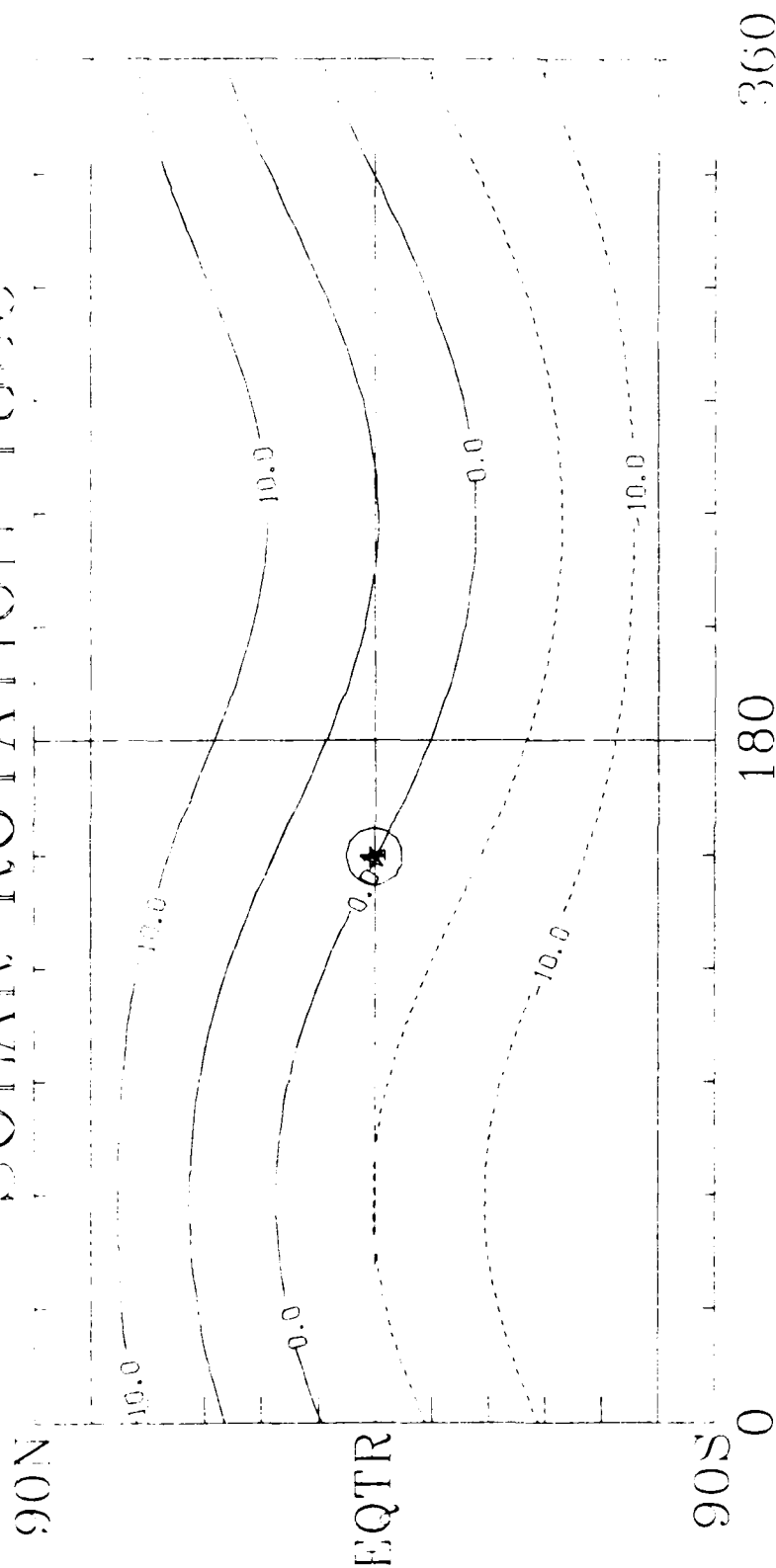
4. Outputs

The parameters chosen in Section 2 determine automatically the locations of the earth and a specific solar flare in our coordinate system, namely the Heliocentric Equatorial (HEQ) coordinate system, where the zero longitude lies along the intersection line of the solar equatorial plane and the ecliptic. In the following, we shall describe briefly each output. For demonstration purposes, we consider a hypothetical flare which is assumed to be reported by the Boulder Solar Observatory, beginning at 1200 UT on December 8, 1990, the location N00, W00 (namely at the center of the solar disk), reaching the maximum intensity at 1300 UT, and ending at 1500 UT: the intensity is 2B.

OUTPUT 3

This output shows the projected location of a hypothetical solar flare by a circle on the Stanford source surface map in Carrington

SOLAR ROTATION 1836



FLARE STN YYMMDD HHMM MAX END LAT LON IB

1 - B0U 901208 1200 1300 1550 N00 W00 2B

Output 3

CONTINUE FROM -10.000 10 10.000 CONTINUE FROM 0.000 10 10.000

longitude-latitude coordinates (Output 1). Since it is assumed that a flare takes place on the center of the solar disk in our particular example, the center of the sun, the flare and the earth are located on a single solar radial line. Therefore, the projections of both the flare and the earth on the source surface coincide at 1200 UT, December 8, 1990 (Output 3). The observed location of the solar disk is automatically converted to a point in Carrington coordinates by specifying the date and time.

OUTPUT 4a

This output shows the solar current sheet to a distance of 2 AU viewed from the longitude of the earth at the time of the solar flare, at 1200 UT, December 8, 1990. The portion of the orbit of the earth above the sheet can be seen as an elliptical curve. From this output, one can see that the earth is located above the current at the time of the flare. The relative location of the earth with respect to the heliospheric current sheet is useful in predicting changes of the IMF angle ϕ .

OUTPUT 4b

This output is optional and shows the solar current sheet to a distance of 5 AU.

OUTPUT 5

Equatorial plane plots of the disturbed IMF are designed to monitor the relative location of the interplanetary disturbance and the earth every six hours after flare onset as the shock wave propagates outward from the sun. The radius of the plots extend to 2 AU. The location of the earth is specified by the * mark. Space probe locations (if any) can be indicated by P1, P2, etc. If a deep space probe at some point between the sun and the earth is available, the disturbed solar wind quantities at the spacecraft location can be predicted and compared with the spacecraft observations to calibrate them well before the expected disturbance arrives at the earth.

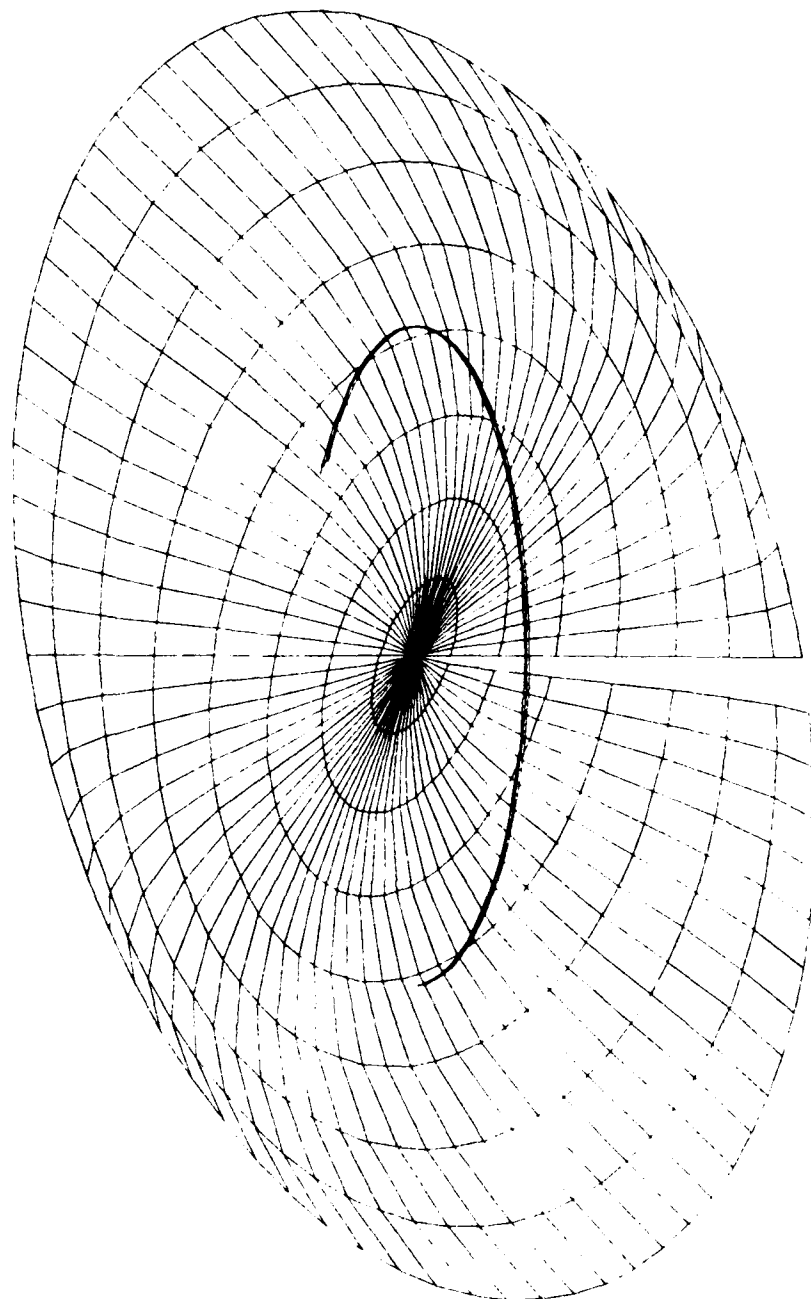
The forecaster will be able to see Output 5 on a CRT screen, so that he can infer that the shock wave will arrive at the earth within a few hours after the onset of this particular flare. In this particular example, the flare occurred at the center of the solar disk (central meridian), so that the center line of the shock wave is directed very closely along the sun-earth line; note that the earth moved by $\sim 1.5^\circ$ after flare onset. The forecaster can see that the shock wave will arrive at the earth between 00 and 06 UT on December 10 in this hypothetical example.

OUTPUT 6

A five-day forecast of solar wind parameters is generated at the earth's location as a function of time. The following parameters are plotted: V = solar wind bulk speed (km/sec); N = solar wind number density (cm^{-3}); B = IMF magnitude (nT); θ = the IMF latitude angle

Rotation #1836

R= 2 AU



Output 4a

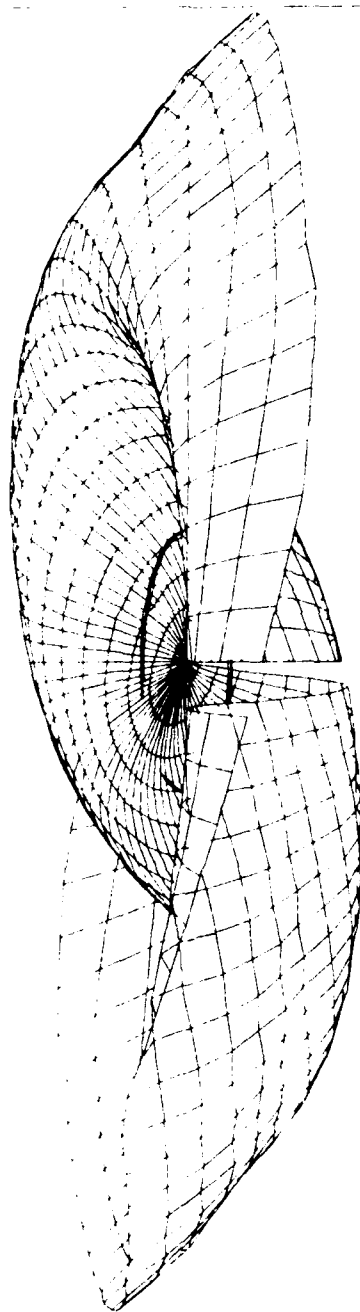
MLAT = 0°

LONG = 0°

LAT = 20°

Rotation = 18.36

R = 5 AU



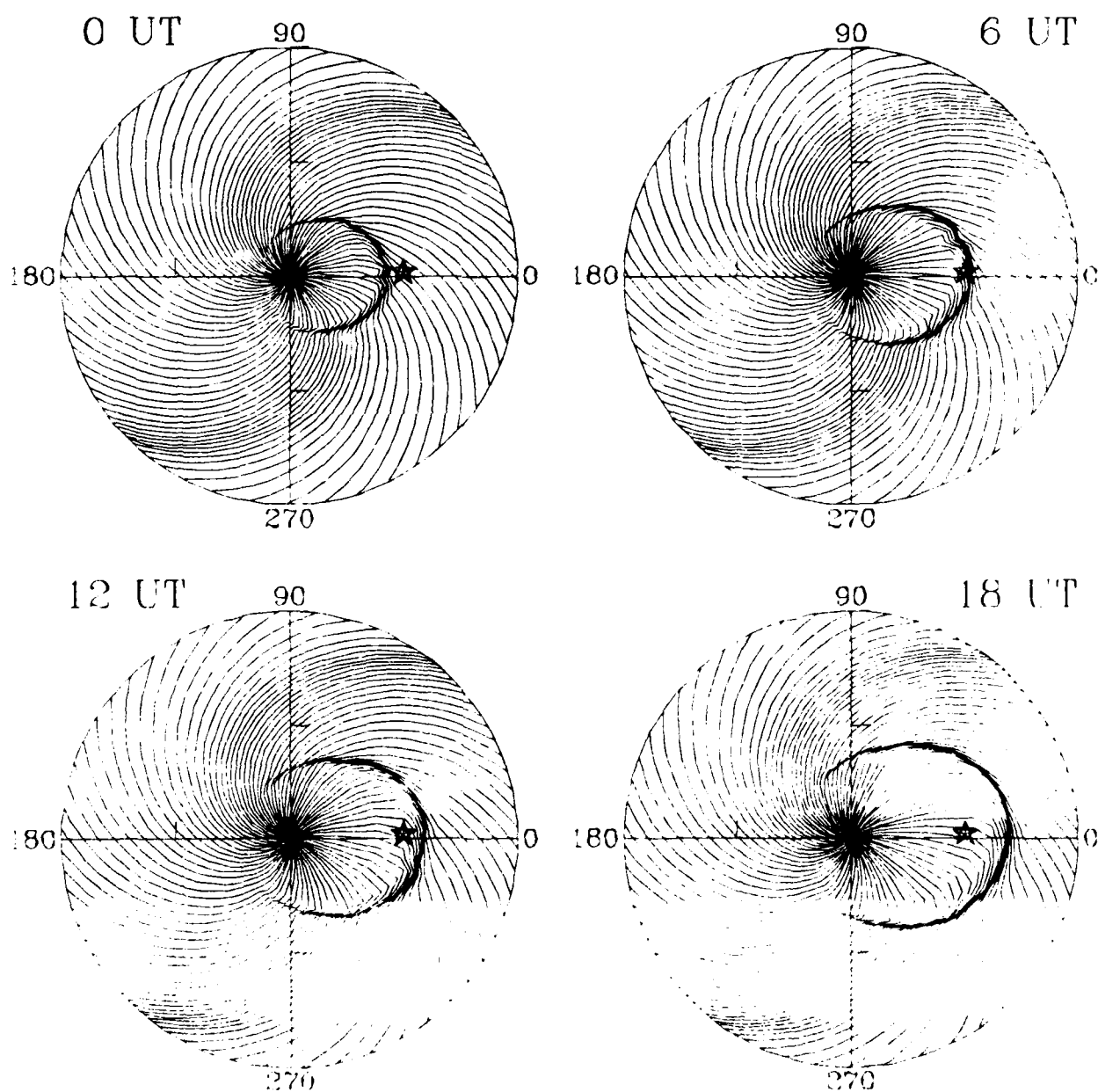
MLAT = 0°

LONG = 0°

LAT = 20°

Output 4b

Ecliptic Plane
2 AU
DEC. 10, 1990



Output 5

(angle the IMF vector makes with the x-y plane) (degrees); ϕ = the azimuthal angle of the IMF vector (degrees).

The forecaster will be able to see Output 6 on a CRT screen and can predict not only the exact arrival time, but also how the quantities V , N , B , θ , ϕ) will change as a function of time. By the time the shock reaches the earth, it develops into the forward and reverse shocks in this particular case, as one can see from a double peak of the speed. The impulsive increase of both the density and the IMF magnitude B are confined in the two shocks. In this particular example, changes of the IMF angle θ are negative and large. The IMF angle ϕ changes from 135° to 315° , indicating the passage of the heliospheric currents. In general, changes of the angle θ are much more complex and depend greatly on the relative location between the flare and the earth (longitude and latitude).

OUTPUT 6a

Plots (V , N , B , θ , ϕ) are produced at specified space-probe locations between the sun and the earth. This particular output allows us to calibrate results from the solar wind code by comparing the predicted values with observed values. For example, if a Venus orbiter is located near the sun-earth line, this output may be useful.

OUTPUT 6b

Plots (V , N , B_x , B_y , B_z) are also produced at specified space-probe locations between the sun and the earth in order to calibrate the solar wind code by comparing the predicted parameters with observed values.

OUTPUT 7

This output is designed for the forecaster to predict how the expected geomagnetic storm develops as a function of time. The following quantities are plotted as a function of time at the Earth's location:

- (1) ϵ = the solar wind-magnetosphere dynamo power.
- (2) ϕ_p = the total potential drop across the polar cap.
- (3) Dst = the average decrease of the horizontal component at the equator (a measure of the ring current intensity).
- (4) AE = the auroral electrojet index.
- (5) U_I = the total energy dissipation rate in the polar ionosphere.
- (6) ΔT_∞ = an increased amount of temperature in the auroral thermosphere.

The following two quantities are also available on demand:

- (7) K_p = the planetary (3-hourly) magnetic index
- (8) ap = the linearized planetary magnetic index T_∞ .

Output 7 shows an example of the predicted ϵ , the potential drop ϕ_{pc} , $Dst(CALDST)$, $AE(CALAE)$, U_I and ΔT_∞ . In this particular case, ϵ increases sharply during the first six hours of December 10, 1990. Then

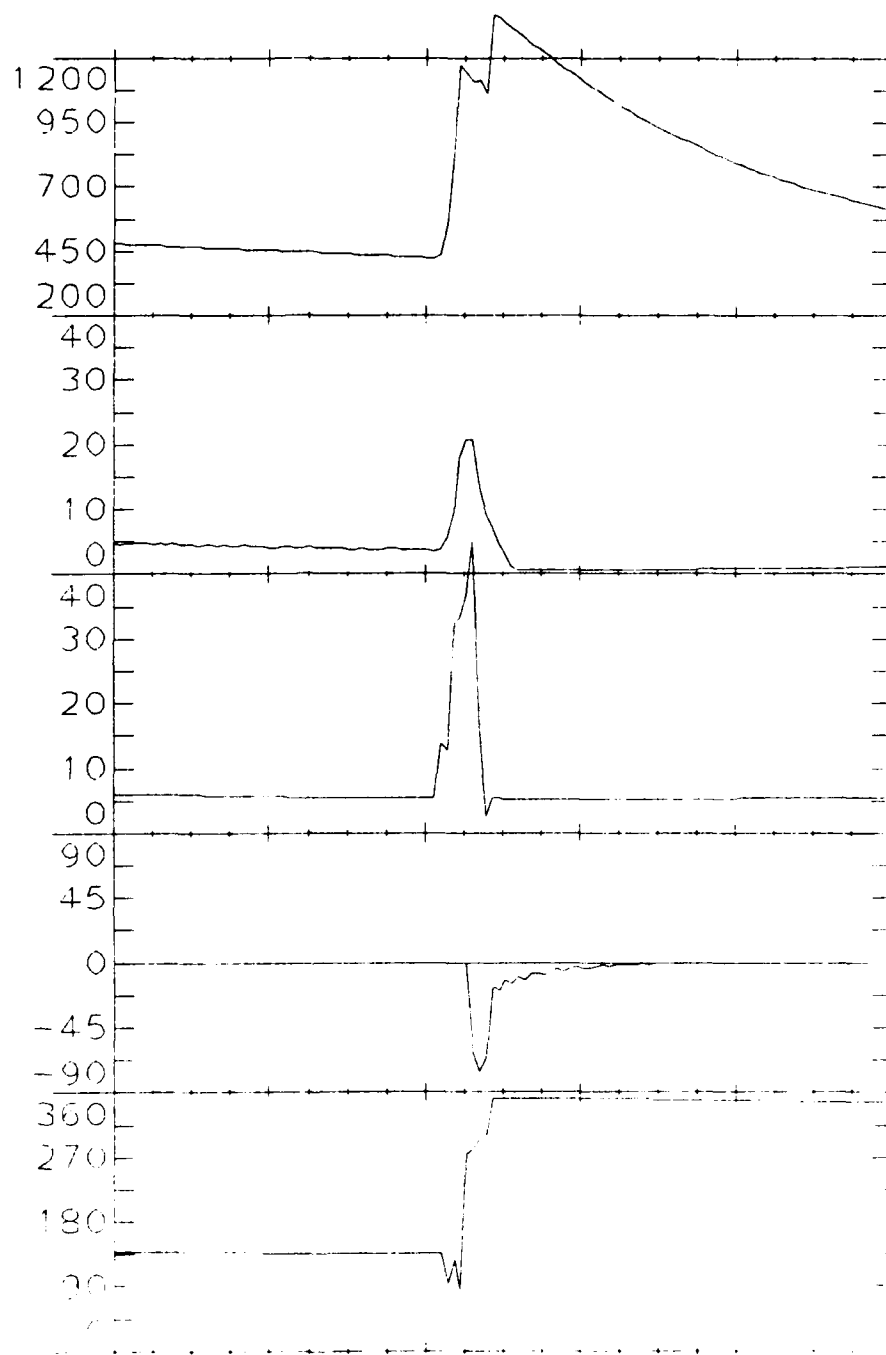
VEL
(Km/Sec)

Dens
(CM⁻³)

/B/
(nT)

⊙
(°)

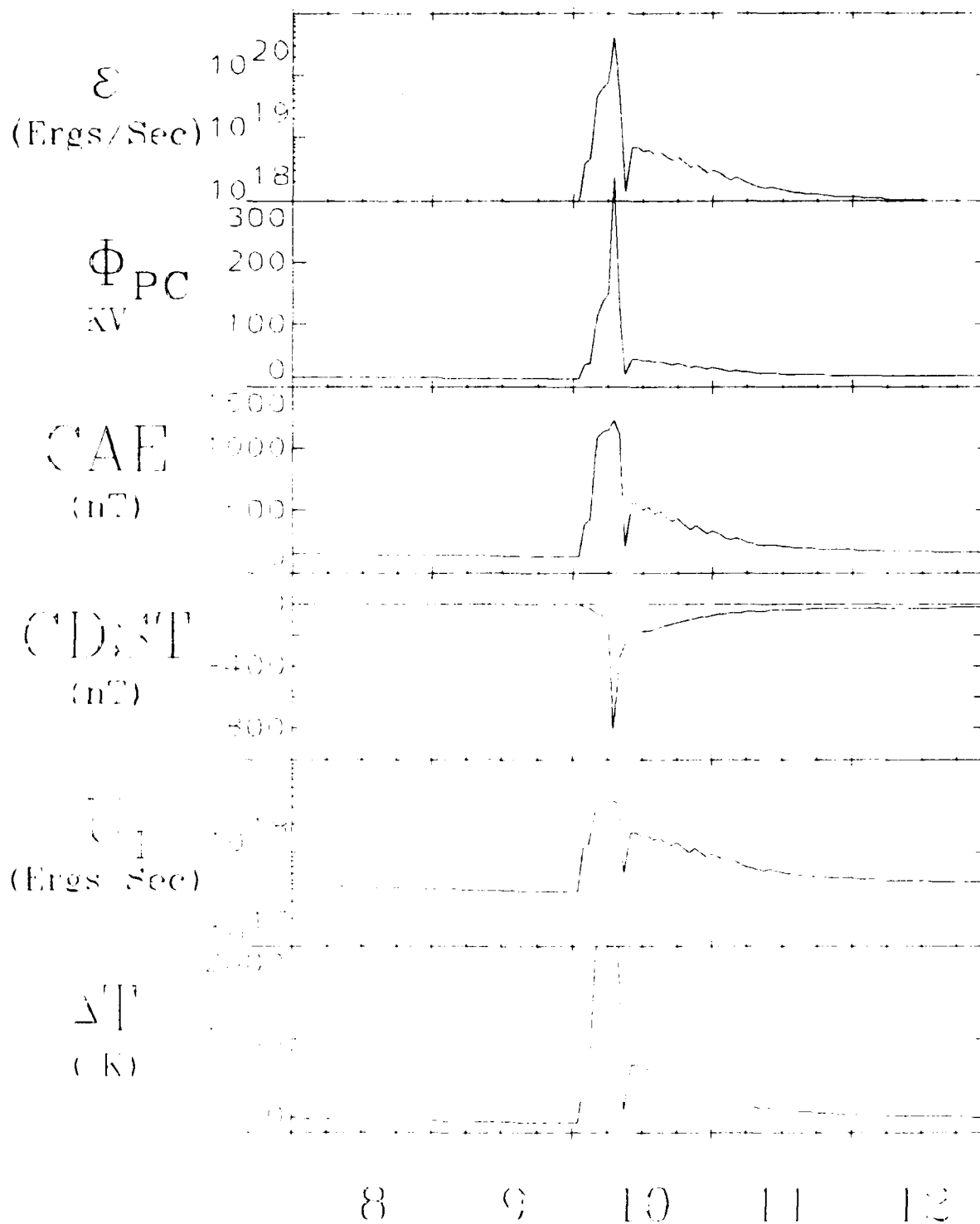
⊙
(°)



8 9 10 11 12

DEC. , 1990

Output 6



DEC. 1990

Output 7

it decreases rather rapidly from ~07 to 09 UT and slowly afterward. The storm 'ends' by 1200 UT on December 12. As expected, the other quantities varied in similar ways.

Thus, the Output 7 allows the forecaster to predict how the storm will develop in terms of the geomagnetic indices AE and Dst as a function of time. The last two quantities are important also in accessing an increase of atmospheric drag which will be experienced by satellites. The above quantities depend greatly on the IMF angle θ which often has most complex changes, so that the resulting storm development is most often much more complex than the example shown here.

OUTPUT 8

Output 8 provides the geometry of the open field line region every three hours after the arrival of the shock wave at the earth (namely, the storm sudden commencement). If an intense solar electron event is expected, this output will be useful in predicting the geometry of the bombardment area by energetic solar electrons. At 00 and 03 UT on December 10, the polar cap size is normal. A slight asymmetry with respect to the noon-midnight meridian is produced by the IMF B_y component. At 06 UT, the polar cap size increases, and the asymmetry becomes opposite to that at 00 and 03 UT; the IMF B_y component changes the sign. The geometry of the solar proton entry area is known to be appreciably longer than that of the electrons. Output 7 information should be available to astronauts in a polar orbiting shuttle. It may be convenient to note that the entry area of solar protons is appreciably larger than that of solar electrons.

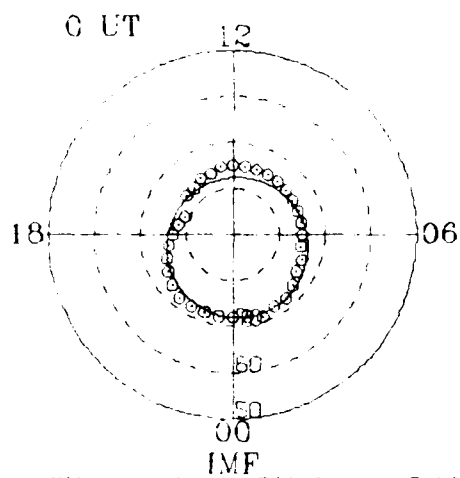
OUTPUT 9

Output 9 provides roughly the geometry of the auroral oval every three hours after the arrival of the shock wave at the earth (namely, the sudden commencement). The size of the oval is quantified in terms of the Q index (a quarter-hourly Kp index). Output 9 shows a sample of the CRT display oval during the storm. One can see that the oval is enlarged considerably at 04 and 07 UT, but is contracted by 10 UT. In the future, the auroral distribution should be adjusted for the Dst index.

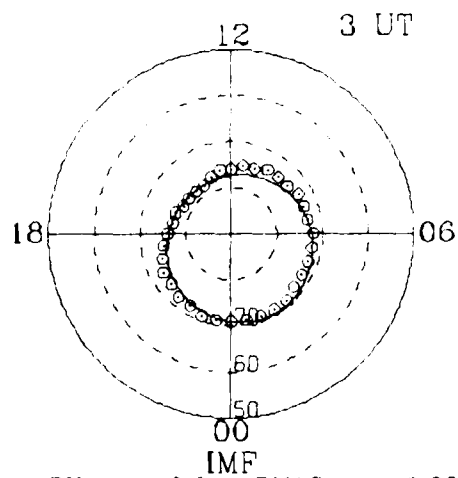
5. Second Generation Scheme

When a large number of codes are integrated to develop a complex scheme, the accuracy and efficiency of the entire scheme is determined by the weakest code component. We list some of the most important improvements to be made on the basis of future studies.

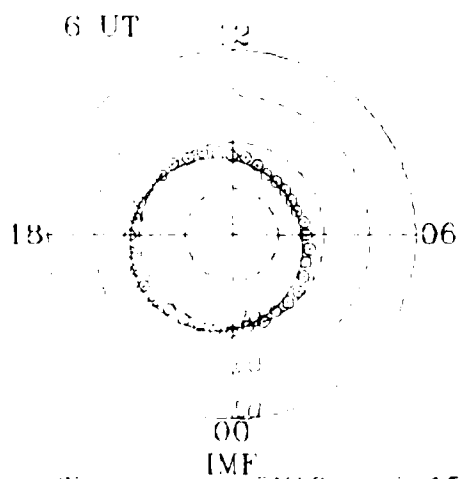
DEC. 10, 1990



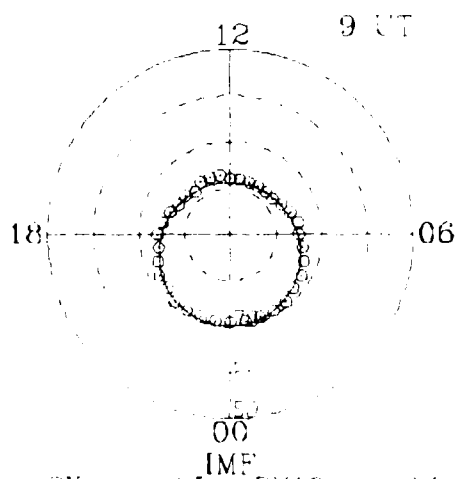
BX= -3.8 BMAG= 5.38
 BY= 3.8 THETA= -0.02
 BZ= 0.0 PHI= 134.90



BX= -0.8 BMAG= 12.88
 BY= 12.9 THETA= 0.00
 BZ= 0.0 PHI= 93.49



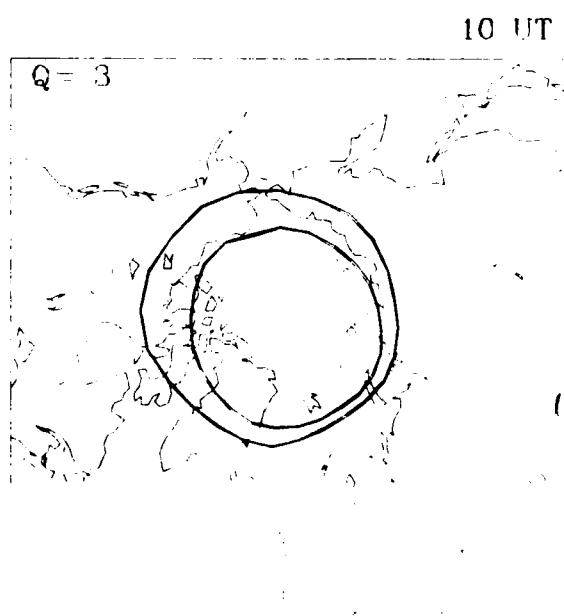
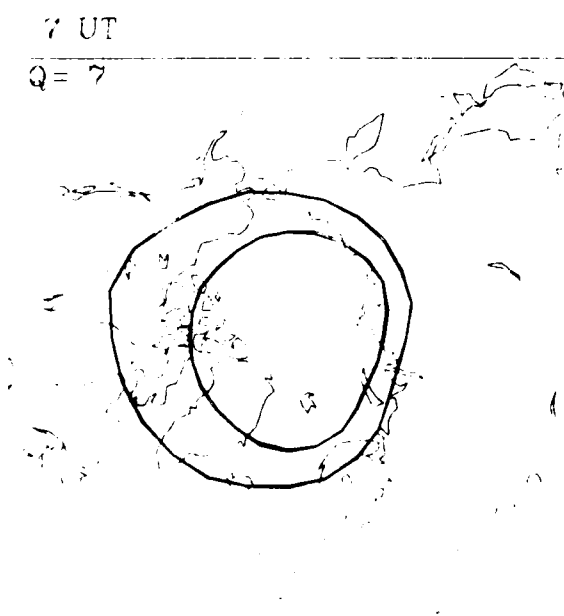
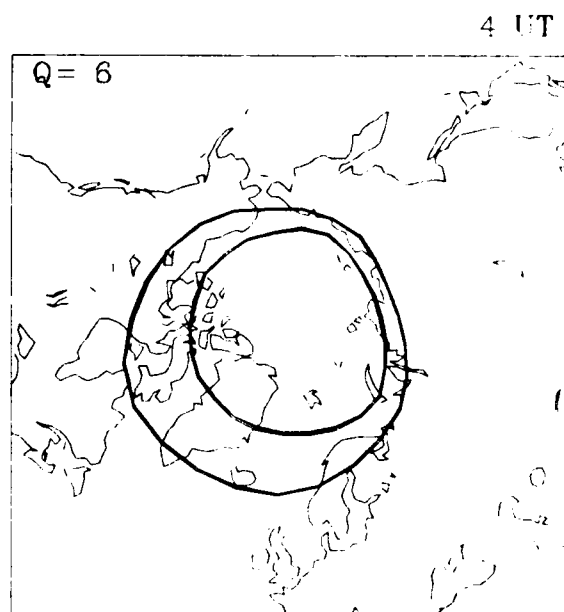
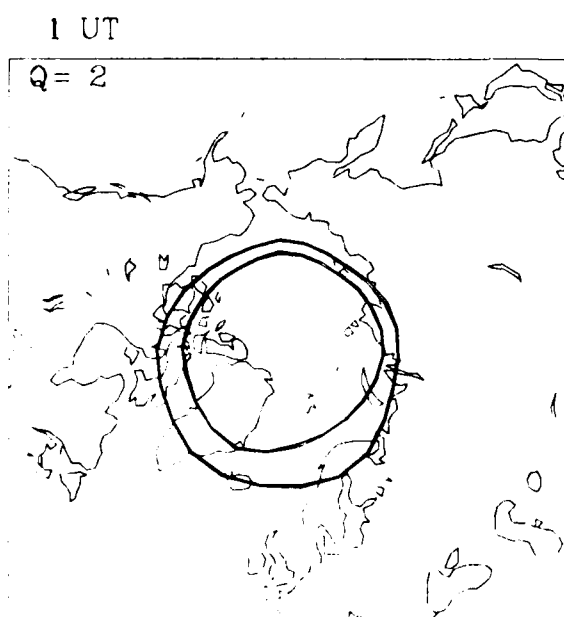
BX= 3.4 BMAG= 36.75
 BY= 3.3 THETA= 0.03
 BZ= 0.0 PHI= 274.32



BX= 0.5 BMAG= 2.68
 BY= 0.9 THETA= 66.38
 BZ= 0.0 PHI= 209.15

Output 8

DEC. 10, 1990



Output 9

(A) IMF B_z component

The weakest part in the first generation scheme lies in properly modeling variations of the north-south component (B_z) of the IMF. This particular subject has fallen into the gap between two disciplines, solar physics and magnetospheric physics, so that there so far have been only a few observational and theoretical papers to guide us in developing our code for this particular purpose.

Basically, a solar flare causes changes of the location of the foot point of magnetic field lines on the source surface. Such changes will be transmitted to interplanetary space and cause changes of the IMF B_z component. At present, our code, based on this principle, adopts one of the simplest changes of the foot point of the field lines. The so-called 'magnetic clouds' could be another cause of the IMF B_z component. Altogether much conceptual development is still needed in understanding IMF B_z changes, as well as associated code developments.

In accomplishing the task described above, we have to make the following efforts for individual solar events.

- (i) Examine solar observations in an attempt to find quantities which are crucial in influencing the IMF B_z component.
- (ii) Model magnetic field variations in the chromosphere and corona during solar flares in order to infer the corresponding magnetic field variations on the source surface.
- (iii) Model the propagation of the disturbances in (ii) to the location of the earth. The opposite approach to (i)-(ii)-(iii) may also be useful. That is to say, on the basis of the observed IMF B_z variations at 1 AU, infer magnetic field variations on the source surface.

(B) Flare parameters

Needless to say that the present determination of the flare parameters is a very tentative one. Much effort is needed to find a suitable value for each parameter. In this respect, it is of great interest to

note that Sheeley et al. (1983) have shown that coronal mass ejections (CMEs) are very highly correlated with long duration soft x-ray events. CMEs are also well correlated with interplanetary shock waves. Therefore, it may well be that τ_F is closely related to the duration τ_D of soft x-ray events (say, $\tau_F \sim 2\tau_D$); both τ_F and the duration of soft x-ray events are much longer than the duration of optical flares. The so-called "halo-type" CMEs observed by the SOLWIND need special attention, because they indicate that a large-scale interplanetary disturbance is directed toward the earth (Howard et al., 1982). An empirical formula for timing the arrival of a solar flare-initiated shock wave has recently been determined by Smart and Shea (1985). Their results should also be incorporated in our determination of V_F in the future.

(C) Magnetosphere-ionosphere coupling

The second weakest part of our scheme is that we rely on several empirical relationships in the second part of the code. They are:

- (i) Determination of the polar cap potential Φ_{pc} by ϵ or AE.
- (ii) Determination of the AE index by ϵ .

These relationships should be replaced by theoretical ones when they become available in the near future.

(D) Ring current formation

In this part of the scheme, we also use a semi-empirical relationship in that it is assumed that 70% of the power ϵ is consumed from the ring current. This empirical relationship should be replaced by a theoretically-based relationship which use ϵ (see Lee et al. (1983)).

5. Concluding Remarks

It is easy to dismiss the present prediction effort by stating that such an attempt is premature at the present time. On the other hand, such an effort can focus our attention to some of the most important issues in solar-terrestrial physics, although they may not necessarily be the most important issues in solar physics or magnetospheric physics. As mentioned earlier, the weakest part of our prediction scheme arises from the fact that causes of IMF B_z changes are not well understood. Thus, these causes are one of the most important unsolved problems in solar-terrestrial physics. Thus, there is absolutely no reason to leave the most important unsolved problem unattended by saying that such efforts are premature.

The first scheme is nothing more than an attempt to demonstrate the basic principle of the modern prediction scheme. We would be more than happy that this report could serve in calling attention to some of the most crucial unsolved problems in solar-terrestrial physics.

Acknowledgements: This work has been funded by Air Force Contract No. F19628-82-K-0035.

References

- Ahn, B.-H., S.-I. Akasofu, Y. Kamide, and J. H. King, Cross-polar cap potential drop and the energy coupling function, J. Geophys. Res., 89, 11028, 1984.
- Akasofu, S.-I., Energy coupling between the solar wind and the magnetosphere, Space Sci. Rev., 28, 121, 1981.
- Akasofu, S.-I., Prediction of development of geomagnetic storms by using the solar wind-magnetosphere energy coupling function ϵ , Planet. Space Sci., 29, 1151, 1982.
- Akasofu, S.-I., and S. Chapman, Solar-Terrestrial Physics, Oxford Univ. Press, 1972.
- Akasofu, S.-I., and M. Roederer, Dependence of the polar cap geometry on the IMF, Planet. Space Sci., 32, 111, 1984.
- Akasofu, S.-I., K. Hakamada, and C. Fry, Solar wind disturbances caused by solar flares: Equatorial plane, Planet. Space Sci., 31, 1435, 1983.
- D'Uston, C., M. Dryer, S. M. Han, and S. T. Wu, Spatial structure of flare-associated perturbations in the solar wind simulated by the two-dimensional numerical MHD model, J. Geophys. Res., 86, 525, 1981.
- Fry, C. G., Three-dimensional structure of the heliosphere: Quiet-time and disturbed periods, Ph.D. Thesis, University of Alaska, Fairbanks, (344 pages) May 1985.
- Gislason, G., M. Dryer, Z. K. Smith, S. T. Wu, and S. M. Han, Interplanetary disturbances produced by a simulated solar flare and equatorially-fluctuating heliospheric current sheet, Astrophys. Space Sci., 98, 149, 1984.

- Hakamada, K., and S.-I. Akasofu, Simulation of three-dimensional solar wind disturbances and resulting geomagnetic storms, Space Sci. Rev., 31, 3, 1982.
- Howard, R. A., D. J. Michels, N. R. Sheeley, Jr., and M. J. Koomen, The observation of a coronal transient directed at earth, Ap. J., 263, 101, 1982.
- Lee, L. C., G. Corrick, and S.-I. Akasofu, On the ring current energy injection rate, Planet. Space Sci., 31, 901, 1983.
- Olmsted, C. D., and S.-I. Akasofu, One-dimensional kinematics of particle stream flow with application to solar wind simulations, Planet. Space Sci. (in press), 1985.
- Perreault, P., and S.-I. Akasofu, Study of geomagnetic storms, Geophys. J. Roy. Astron. Soc., 54, 547, 1978.
- Prölss, G. W., Correlation between upper atmospheric temperature and solar wind conditions, J. Geophys. Res. (in press), 1985.
- Reiff, P. H., R. W. Spiro, and T. W. Hill, Dependence of polar cap potential drop on interplanetary parameters, J. Geophys. Res., 86, 7639, 1981.
- Sheeley, N. R., Jr., R. A. Howard, M. J. Koomen, and D. J. Michels, Associations between coronal mass ejections and soft x-ray events, Ap. J., 272, 349, 1983.
- Smart, D. F., and M. A. Shea, A simplified model for timing the arrival of solar flare-initiated shocks, J. Geophys. Res., 90, 183, 1985.

END

FILMED

1-86

DTIC